GaInAsSb / AlGaAsSb / GaSb Thermophotovoltaic Devices

CA Wang

GaInAsSb/AlGaAsSb/GaSb Thermophotovoltaic Devices

M.I.T. Technical Seminar

4 February 2004

C.A. Wang

Lincoln Laboratory, Massachusetts Institute of Technology

Lexington, MA

TPV-1
CAW 6/1/2004

Viewgraph 1:

Thermophotovoltaic (TPV) devices based on III-V semiconductor alloys with bandgap energies corresponding to the mid-infrared wavelength range 2.2 to 2.5 μm (0.5 to 0.56 eV) are being developed. To date, the highest performing TPV devices in this wavelength range have been achieved for devices based on GaInAsSb and AlGaAsSb alloys lattice matched to GaSb substrates. The first 0.55-eV TPV cells in this materials system were reported at the Third NREL Conference on Thermophotovoltaic Generation of Electricity in 1997. Smaller-bandgap TPV devices have subsequently been reported with concurrent improvements in TPV device performance. This has largely been due to ongoing efforts to understand fundamental processes in materials growth, intrinsic materials properties, and their relationships to TPV device structure design and performance. This work reports some of the fundamental as well as practical issues that have been identified as critical parameters for achieving high performance TPV cells.

Outline

- **Current status of GaInAsSb/AlGaAsSb/GaSb TPV devices**
- **Materials and device fabrication studies**
  - Critical issues for epitaxial growth of GaSb-based materials
  - Materials properties
  - Contact metallization and cell edge treatment
- **TPV device structure improvements**
  - Integrated distributed Bragg reflectors (DBR)
  - Back surface reflector (BSR)
  - New concepts: wafer-bonded TPVs with internal BSR
- **Summary**

Viewgraph 2:

The presentation will discuss several aspects of the development of lattice-matched GaInAsSb TPV devices. The growth of device structures, which consist of GaSb, GaInAsSb and AlGaAsSb layers grown epitaxially on GaSb substrates is first presented. A high degree of control and reproducibility is required for producing materials and device structures with high quality, and this is demonstrated for structures grown by organometallic vapor phase epitaxy (OMVPE). The performance of TPV devices and new structures is presented.

Error

An error occurred while processing this page. See the system log for more details.

Error

An error occurred while processing this page. See the system log for more details.

Error

An error occurred while processing this page. See the system log for more details.

Error

An error occurred while processing this page. See the system log for more details.

Error

An error occurred while processing this page. See the system log for more details.

Error

An error occurred while processing this page. See the system log for more details.

Error

An error occurred while processing this page. See the system log for more details.

Error

An error occurred while processing this page. See the system log for more details.

Error

An error occurred while processing this page. See the system log for more details.

Error

An error occurred while processing this page. See the system log for more details.

Error

An error occurred while processing this page. See the system log for more details.

Error

An error occurred while processing this page. See the system log for more details.

Error

An error occurred while processing this page. See the system log for more details.

Error

An error occurred while processing this page. See the system log for more details.

Error

An error occurred while processing this page. See the system log for more details.

Error

An error occurred while processing this page. See the system log for more details.
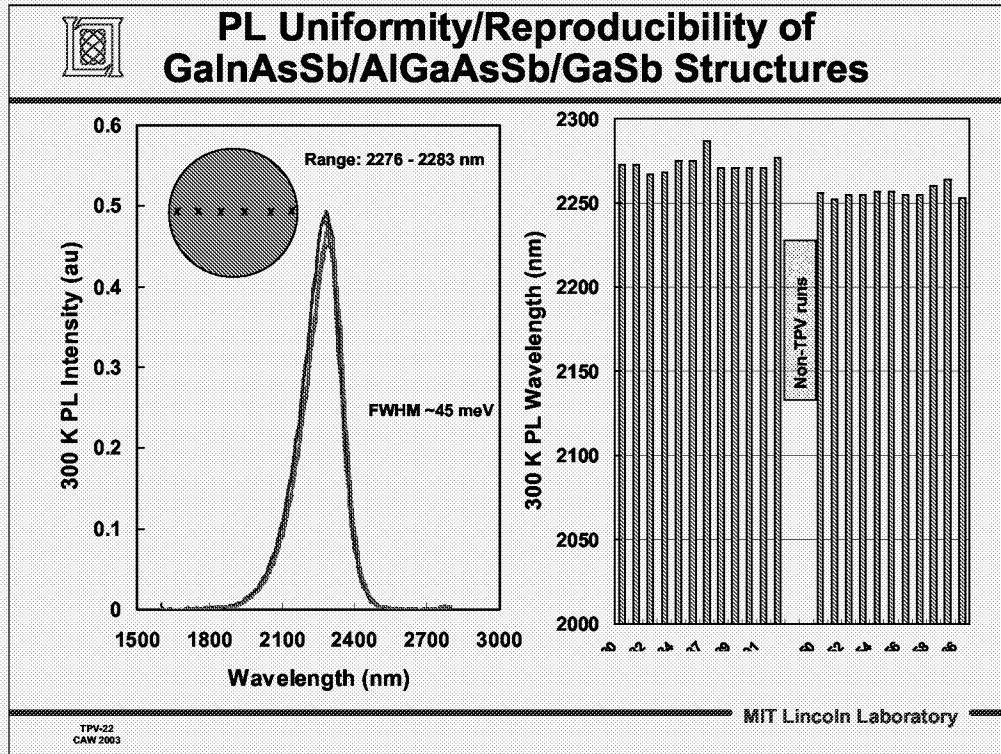
Error

An error occurred while processing this page. See the system log for more details.

Error

An error occurred while processing this page. See the system log for more details.

Error

An error occurred while processing this page. See the system log for more details.

PL Uniformity/Reproducibility of GaInAsSb/AlGaAsSb/GaSb Structures

Range: 2276 - 2283 nm

FWHM ~45 meV

300 K PL Intensity (au)

Wavelength (nm)

300 K PL Wavelength (nm)

Non-TPV runs

TPV-22
CAW 2003

MIT Lincoln Laboratory

Viewgraph 22:

Macroscopic uniformity was also achieved for GaInAsSb grown under conditions to minimize phase separation. The uniformity and reproducibility of GaInAsSb structures is shown in this viewgraph. The PL emission wavelength (alloy composition) and intensity is very uniform over a 2-inch-diameter substrate. Two separate series of growth runs indicate reproducibility in PL wavelength.
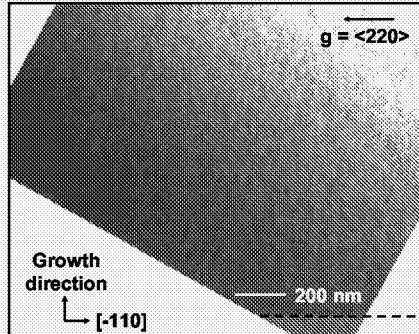
Error

An error occurred while processing this page. See the system log for more details.

Effect of Alloy Composition

0.6-eV $Ga_{0.9}In_{0.1}As_{0.09}Sb_{0.91}$

0.5-eV $Ga_{0.8}In_{0.2}As_{0.18}Sb_{0.82}$

g = <220>

g = <220>

Growth direction

[-110]

200 nm

200 nm
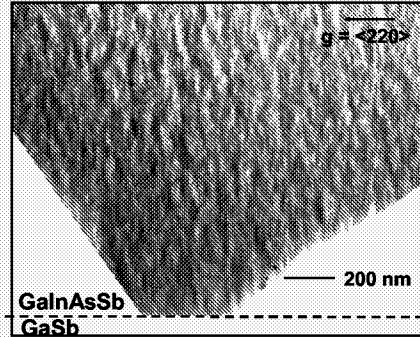
GaInAsSb
GaSb

Further into miscibility gap

[110] Cross-section
(001) 6° → (1-11)B, T = 525 °C

MIT Lincoln Laboratory

TPV-24
CAW 2003

Viewgraph 24:

This viewgraph shows cross-section TEM images of GaInAsSb of different alloy compositions. As the alloy composition penetrates further into the misibility gap, the TEM contrast increases due to spinodal decomposition.

Effect of Alloy Composition
(-1-11)A step edge

$Ga_{0.9}In_{0.1}As_{0.09}Sb_{0.91}$ $Ga_{0.85}In_{0.15}As_{0.14}Sb_{0.86}$ $Ga_{0.81}In_{0.19}As_{0.17}Sb_{0.83}$

GaInAsSb
GaSb

Further into miscibility gap

T_g = 575 °C
(001) 2°→(-1-11)A

200 nm
g = <220>

MIT Lincoln Laboratory

TPV-25
CAW 2003
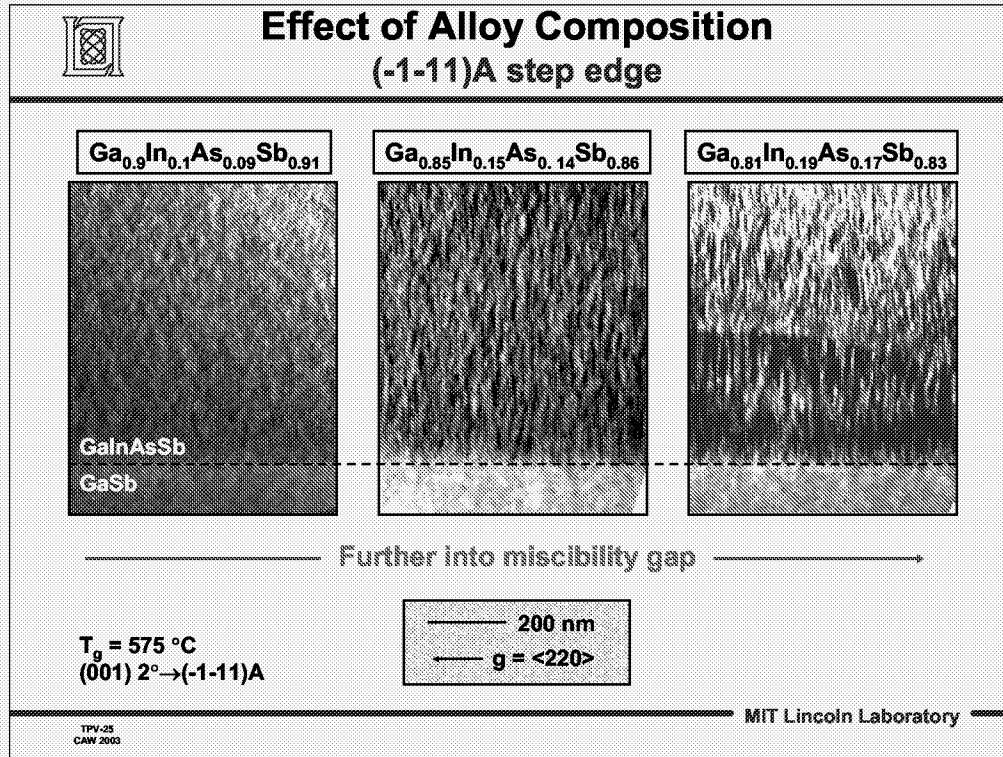
Viewgraph 25:

This viewgraph shows TEM cross-sections of alloys grown on (001) substrates miscut 2° toward (1-11)A. Contrast modulations increase as the alloy composition moves further into the miscibility gap.

Effect of Alloy Composition
(101) step edge

$Ga_{0.89}In_{0.11}As_{0.09}Sb_{0.91}$

$Ga_{0.81}In_{0.19}As_{0.17}Sb_{0.83}$

GaInAsSb
GaSb

Further into miscibility gap

$T_g = 575\,°C$
(001) 2°→(101)

200 nm
g = <220>

MIT Lincoln Laboratory

TPV-26
CAW 2003
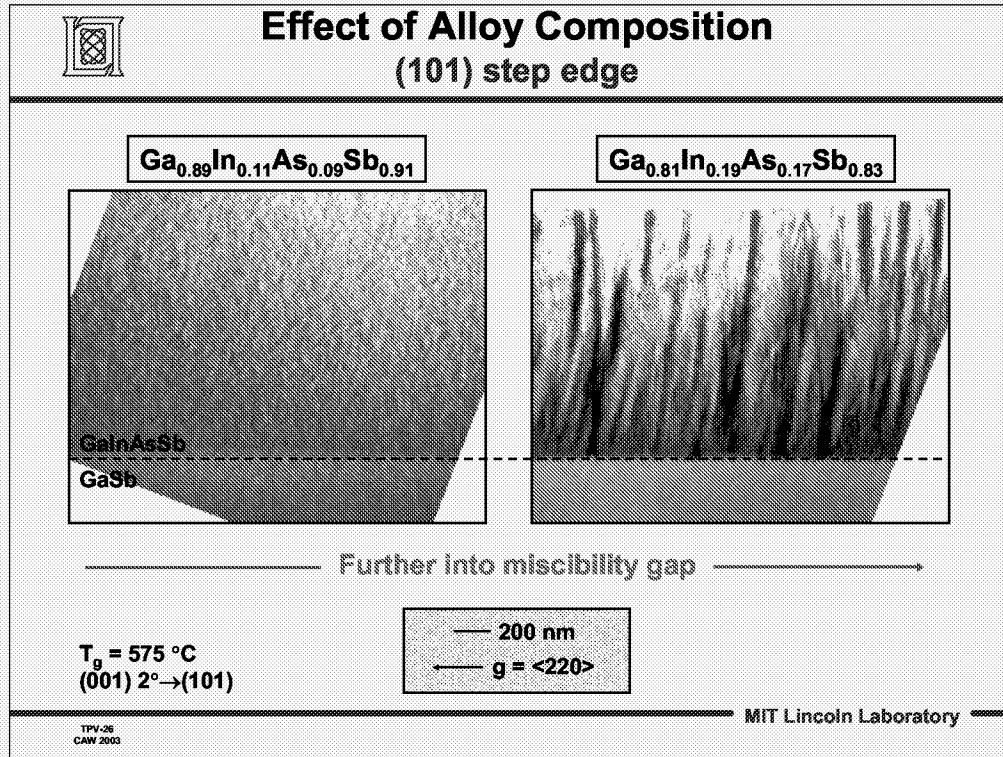
Viewgraph 26:

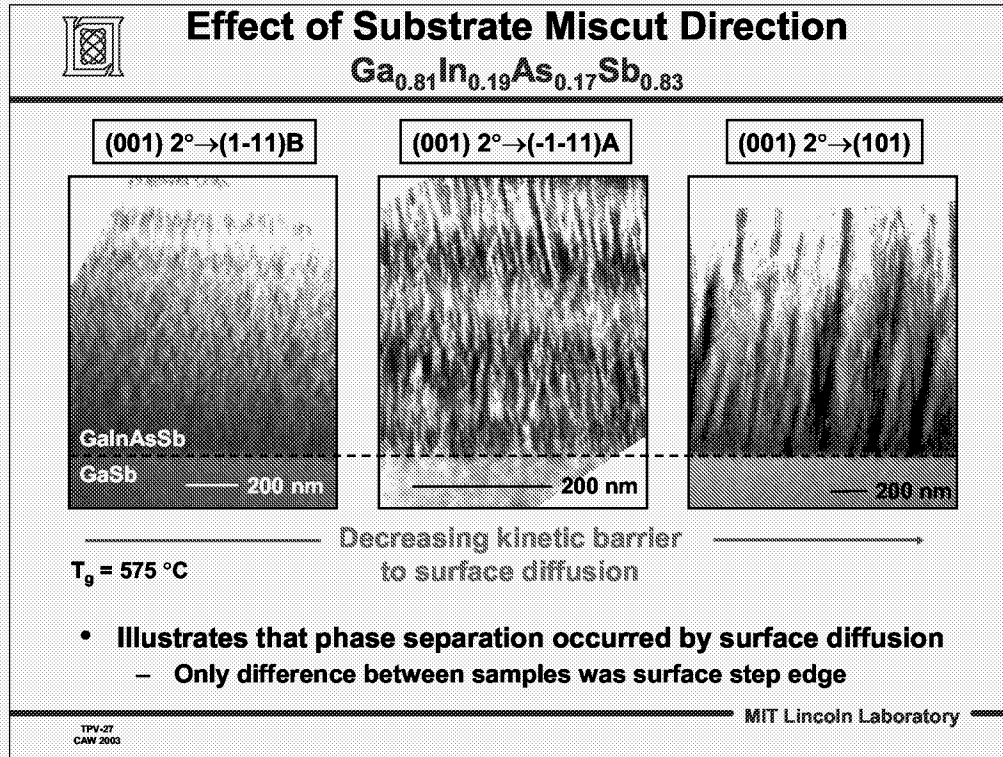This viewgraph shows TEM cross-sections of alloys grown on (001) substrates miscut 2° toward (101). Contrast modulations increase as the alloy composition moves further into the miscibility gap. Note that the contrast in the higher alloy layer is greater in this viewgraph compared to the previous two viewgraphs.

Effect of Substrate Miscut Direction
$Ga_{0.81}In_{0.19}As_{0.17}Sb_{0.83}$

(001) 2°→(1-11)B   (001) 2°→(-1-11)A   (001) 2°→(101)

GaInAsSb
GaSb   200 nm   200 nm   200 nm

Decreasing kinetic barrier
$T_g = 575\ °C$ to surface diffusion

- **Illustrates that phase separation occurred by surface diffusion**
  - **Only difference between samples was surface step edge**

TPV-27
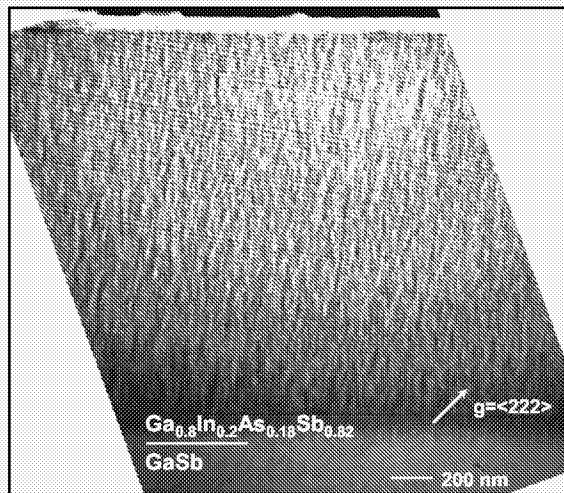CAW 2003   MIT Lincoln Laboratory

Viewgraph 27:

This viewgraph shows TEM cross-sections of alloys grown on the various miscut substrates. All the layers have a similar alloy composition, and were grown under the same conditions of growth rate, growth temperature and miscut angle. However, they show various contrast modulations. Since the only difference is miscut direction, the bonding/chemistry at step edge is very important in determining phase separation. These results show that phase separation occurs by surface diffusion. Since the adatom diffusion and incorporation is anisotropic, the miscut direction can be critical in determining the extent of phase separation.
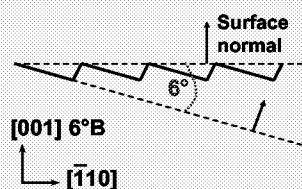
Self-Organized Tilted Natural Superlattice (NSL) in 0.5-eV GaInAsSb/GaSb

- **NSL forms at onset of growth and continues throughout**
- **20 nm period**
- **NSL has 10° tilt**

Step-flow growth

Surface normal

6°

[001] 6°B

[$\bar{1}$10]

$Ga_{0.8}In_{0.2}As_{0.18}Sb_{0.82}$

GaSb

g=<222>

200 nm

[110] cross-section
(001) 6° → (1-11)B, T = 525 °C
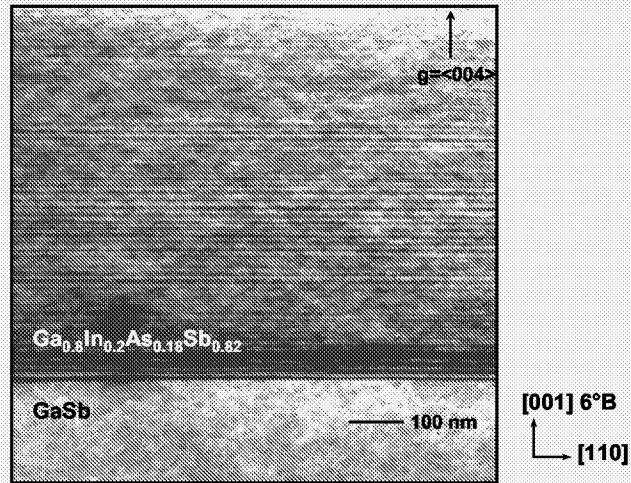
MIT Lincoln Laboratory

TPV-28
CAW 2003

Viewgraph 28:

An interesting self-organized natural superlattice(NSL) was observed in GaInAsSb materials that also showed spinodal-like contrast modulations. This viewgraph contains a cross-section TEM image illustrating the NSL in the GaInAsSb epilayer. The image was obtained using a dark-field, <222> 2-beam condition. The vertical composition modulation exhibits two forms – a 0° variant that is parallel to the epilayer/substrate interface, and a 10° variant that is tilted 10° with respect to the surface normal.

The observed contrast arises from a very small degree of strain associated with a modulation in composition in the vertical direction. The contrast, and thus compositional differences between the layers, depended on the growth conditions and the alloy composition. It was found that the vertical composition modulation can be reduced or enhanced by varying the growth conditions.

Cross-section TEM suggests that GaInAsSb self-organizes at the onset of growth and maintains a consistent periodicity throughout several microns of deposition. A particularly remarkable feature of the vertical modulation is the ordering of atoms to produce a layered structure that is tilted 4° in addition to the miscut angle of the (001) substrate surface plane.

NLS in 0.5-eV GaInAsSb/GaSb

$Ga_{0.8}In_{0.2}As_{0.18}Sb_{0.82}$

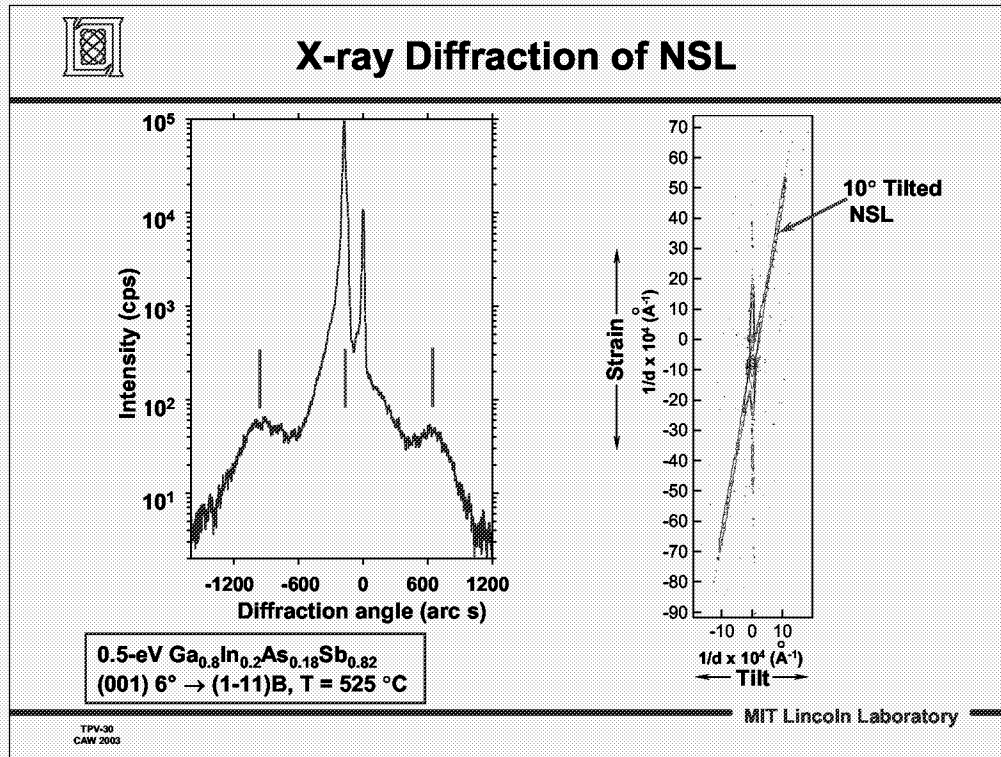GaSb

$g=<004>$

[001] 6°B

[110]

——— 100 nm

[-110] cross-section
(001) 6° → (1-11)B, T = 525 °C

MIT Lincoln Laboratory

TPV-29
CAW 2003

Viewgraph 29:

This viewgraph contains the orthogonal cross-section TEM image illustrating the self-organized NSL in the GaInAsSb epilayer. In this cross-section, the self-organized NSL is parallel to the growth surface.

X-ray Diffraction of NSL

0.5-eV $Ga_{0.8}In_{0.2}As_{0.18}Sb_{0.82}$
(001) 6° → (1-11)B, T = 525 °C

MIT Lincoln Laboratory

TPV-30
CAW 2003

Viewgraph 30:

The NSL was also detected in XRD. The rocking curve on the left shows satellite peaks that are symmetric about the epilayer peak. The reciprocal space map on the right shows the tilted superlattice. The tilt angle can be quantitatively measured in XRD.

Effect of Ga$_{1-x}$In$_x$As$_y$Sb$_{1-y}$ Composition
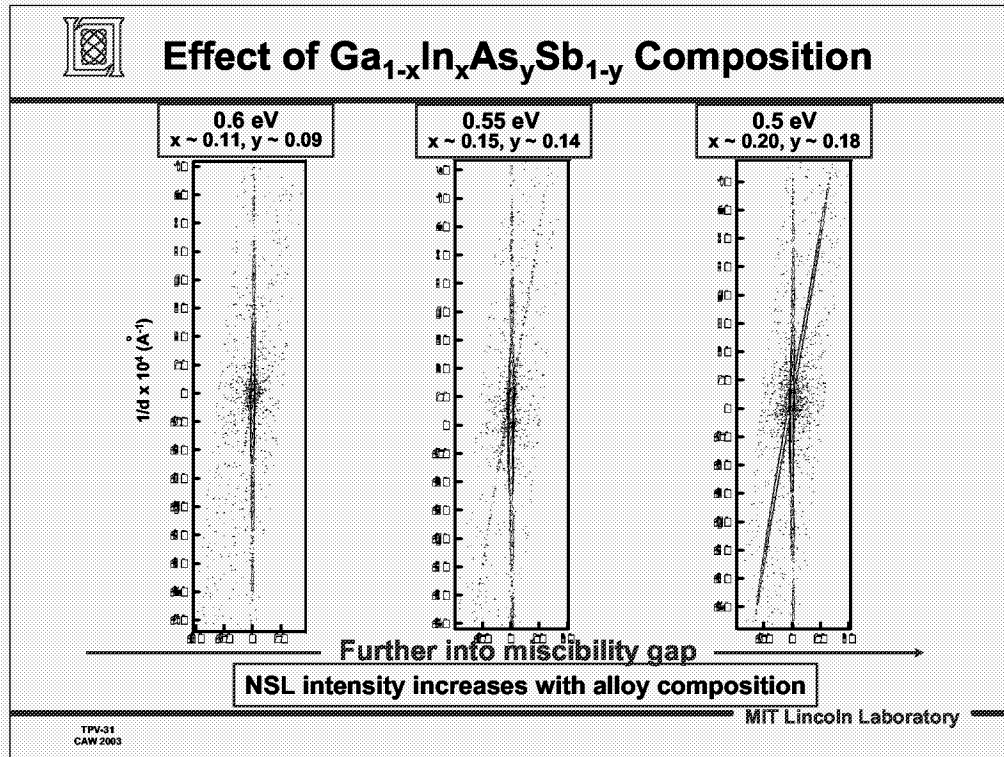
Viewgraph 31:

The reciprocal space maps of three different GaInAsSb alloys show that the intensity of the tilte superlattice increases for the alloys further into the miscibility gap.

Photoluminescence of GaInAsSb

No Tilted Superlattice
0.6-eV GaInAsSb

300 K
4 K

PL Intensity (au)

FWHM = 4.3 meV

ΔE_{4-300K} = 73 meV

0.5   0.6   0.7
Energy (eV)

Tilted Superlattice
0.5-eV GaInAsSb

300 K
4 K

PL Intensity (au)

FWHM = 9.5 meV

ΔE_{4-300K} = 46 meV

0.4   0.5   0.6
Energy (eV)

TPV-32
CAW 2003

MIT Lincoln Laboratory
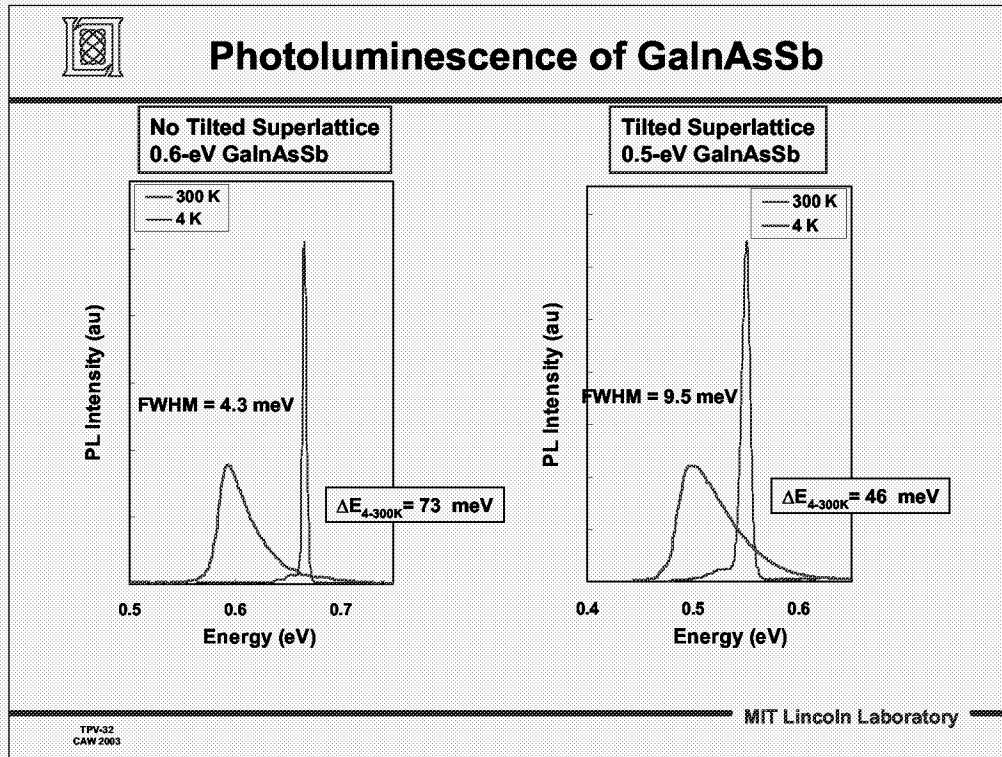
Viewgraph 32:

The microstructure can impact the electro-optical properties of GaInAsSb epilayers. Although composition modulation is expected to increase the PL linewidth because of local variations in alloy composition, the FWHM broadening was minimal as shown in this viewgraph. The sample with weak superlattice contrast has excellent PL properties and the dependence of the PL peak energy on temperature is typical of bulk materials or superlattices with a type-I band alignment.

The sample with strong superlattice contrast exhibits slight FWHM broadening which may also be due to layer thickness variations of the superlattice or spinodal decomposition. The temperature dependence of PL peak energy is similar to what is observed for type-II band alignment.

Tilted NSL and Surface Undulations in GaInAsSb

No Tilted NSL 0.6-eV GaInAsSb

Tilted NSL 0.5-eV GaInAsSb

[-1-10] [1-10]
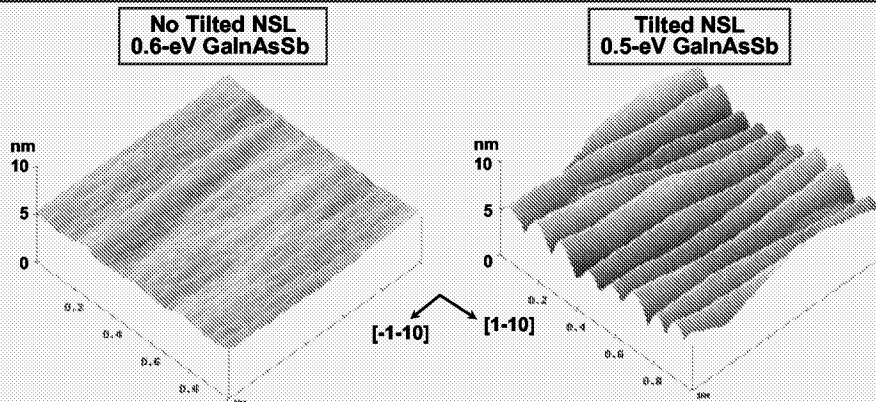
- **Tilted NSL associated with surface undulations**
  - **Undulations aligned along step edges (step-flow growth)**
  - **Amplitude of surface undulation increases with (1) strength of NSL and (2) for alloys deeper in miscibility gap**

Viewgraph 33:

The existence of the tilted NSL was also correlated with surface undulations. Epilayers that did not have the tilted NSL were smooth with surface roughness of typically 2-3 nm, while those with a tilted NSL exhibited periodic surface undulations that are aligned with the step edges of the vicinal substrates. The amplitude of surface undulations increased for alloys further into the misciblity gap. Tilted NSLs were also observed on step-bunched surfaces.

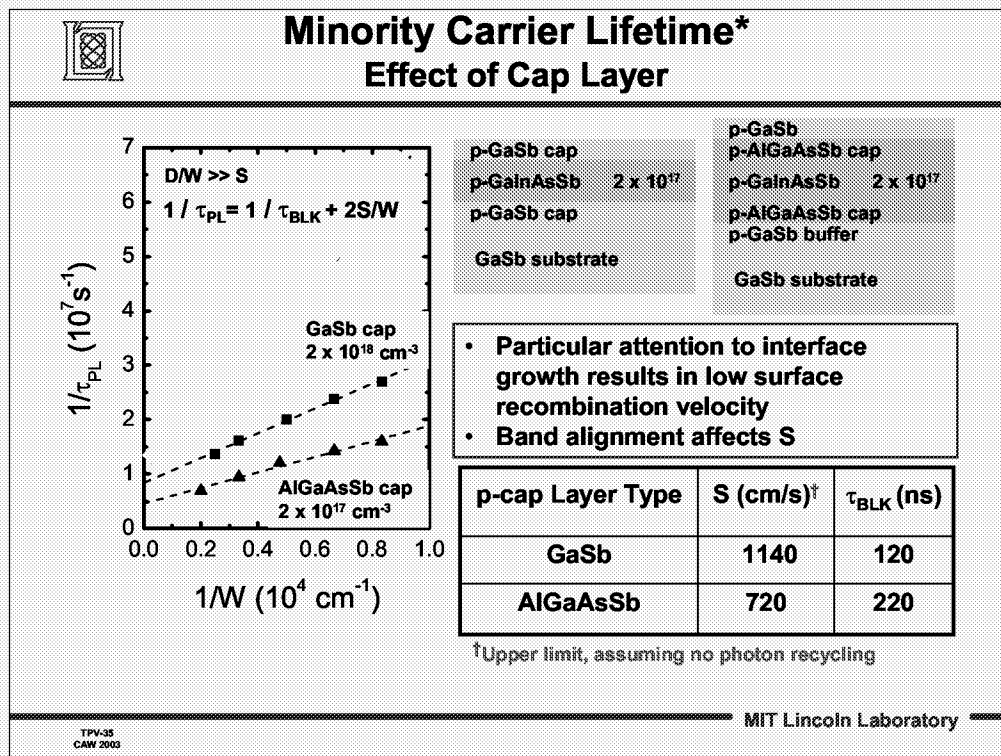## Surface Undulations Coupled to Tilted Superlattice
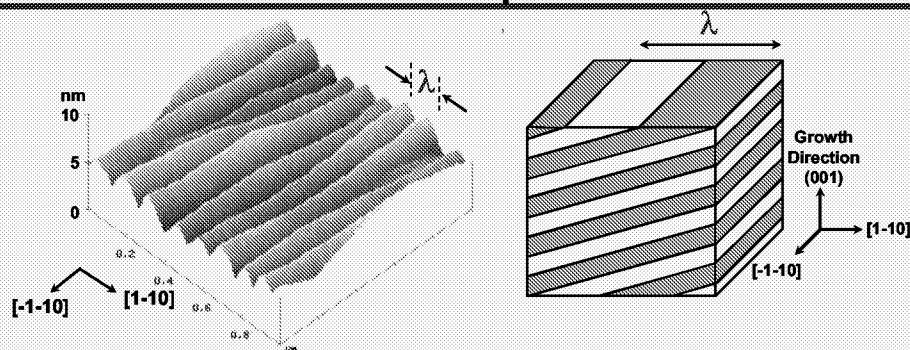
Miscut ∠	NSL period (nm)	NSL Tilt ∠	Calc λ (nm)	AFM λ (nm)
6° (1-11)B	20	10°	115	111
2° (1-11)B	14.6	5.8°	144	143
2° (101)	13.8	6.0°	132	160
2° (111)A	30	0°	∞	No undulation

Viewgraph 34:

The undulation period matches the lateral period of the 10° tilted superlattice when it intersects the surface. Furthermore, data from additional samples indicate that the amplitude of the undulations increases as the alloy composition goes further into the miscibility gap. This suggests that the undulations form on the surface to relieve the local strain from the composition modulation associated with the superlattice. This phenomenon of coupling of compositional and morphological instabilities is well documented in the literature.

$$D/W \gg S$$
$$1 / \tau_{PL} = 1 / \tau_{BLK} + 2S/W$$

GaSb cap
2×10^{18} cm^{-3}

AlGaAsSb cap
2×10^{17} cm^{-3}

Plot: $1/\tau_{PL}$ (10^7 s^{-1}) vs $1/W$ (10^4 cm^{-1})

Structure (left):
p-GaSb cap
p-GaInAsSb 2×10^{17}
p-GaSb cap
GaSb substrate

Structure (right):
p-GaSb
p-AlGaAsSb cap
p-GaInAsSb 2×10^{17}
p-AlGaAsSb cap
p-GaSb buffer
GaSb substrate

- Particular attention to interface growth results in low surface recombination velocity
- Band alignment affects S

p-cap Layer Type	S (cm/s)†	τ_{BLK} (ns)
GaSb	1140	120
AlGaAsSb	720	220

†Upper limit, assuming no photon recycling

MIT Lincoln Laboratory

TPV-35
CAW 2003

Viewgraph 35:

Minority carrier lifetime of specially grown structure were measured by time-resolved PL at Stonybrook. This viewgraph shows the dependence of $1/\tau_{PL}$ on $1/W$ for GaInAsSb heterostructures with different cap layers. All three plots demonstrate a linear dependence consistent with the equation. The structures with undoped (p = 1×10^{16} cm^{-3}) GaSb cap layers resulted in the highest S of 3100 cm/s. In structures with p-GaSb cap layers doped to 2×10^{18} cm^{-3}, S was substantially smaller at 1140 cm/s. Thus, the use of a heavily doped cap layer makes it possible to suppress interfacial recombination. S was further reduced to 720 cm/s for structures with AlGaAsSb cap layers. The smallest S was 380 cm/s for undoped GaInAsSb with AlGaAsSb cap layers.
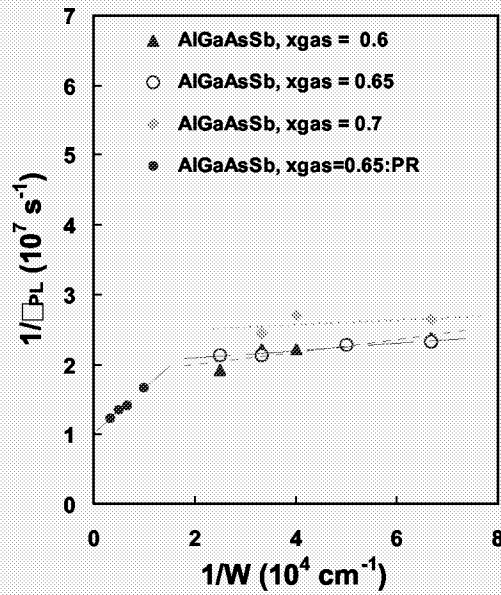
Minority Carrier Lifetime*
Effect of GaInAsSb Doping

p=2x10^{17}cm^{-3}

1x10^{17}

1x10^{16}

$1/\tau_{PL}$ (10^{7}s^{-1})

1/W (10^{4}cm^{-1})

p-GaSb cap   1 x 10^{16}
p-GaInAsSb   p-varied
p-GaSb cap   1 x 10^{16}

GaSb substrate

$D/W \gg S$ $1 / \tau_{PL} = 1 / \tau_{BLK} + 2S/W$

GaInAsSb doping (cm^{-3})	S (cm/s)	τ_{BLK} (ns)
2 x 10^{17}	3100	100
1 x 10^{17}	2300	370
1 x 10^{16}	1900	900

MIT Lincoln Laboratory

TPV-36
CAW 2003
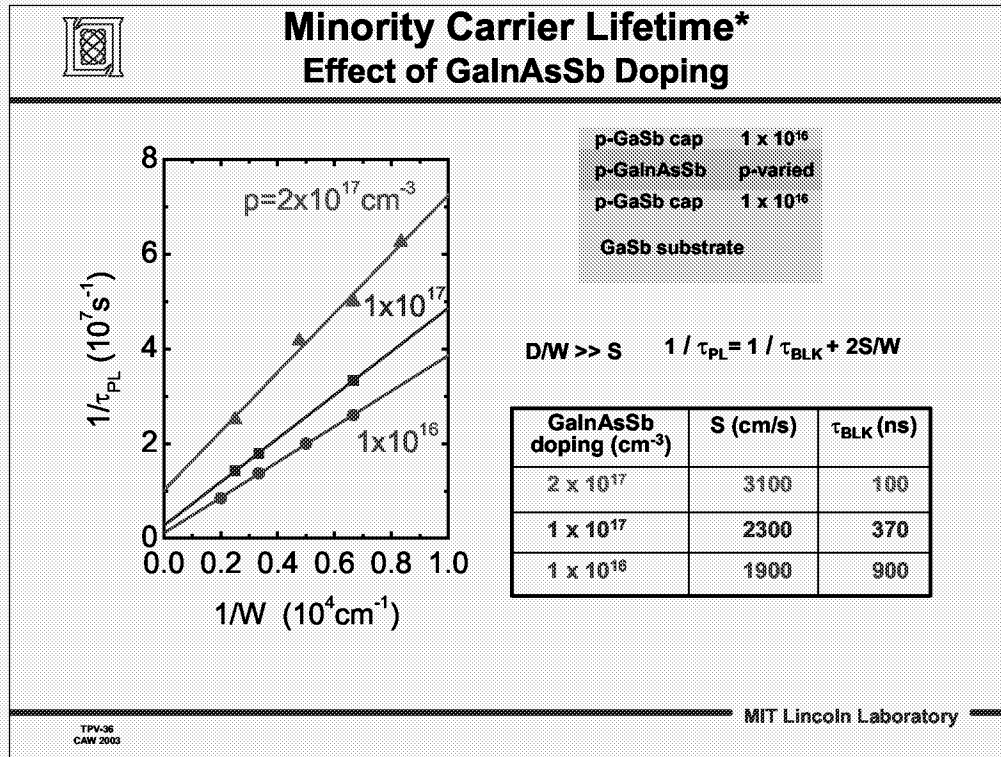
Viewgraph 36:

The electron lifetime of p-GaInAsSb doped at various levels was measured by time resolved PL. Heterostructures with different GaInAsSb thicknesses were grown with nominally undoped p-GaSb buffer and capping layers in order to separate the contributions of bulk and interfacial recombination processes. Due to the fast electron diffusion, $D/W \gg S$, the commonly used expression shown above was employed. Plotting the inverse PL decay versus inverse structure thickness reveals a linear dependence with a slope of *2S*.

The plot on the left shows the data for structures with different doping levels in the GaInAsSb layer: 1 x 10^{16}, 1 x 10^{17} and 2 x 10^{17} cm^{-3}. The radiative part of recombination depends on W due to the effect of reabsorption (photon recycling) and therefore contributes to the measured slope and affects the offset value. For structures with p = 1 x 10^{16} cm^{-3} the contribution of the photon recycling is negligible, so the offset of 900 ns for undoped structures can be used as a lower estimate of the non-radiative bulk lifetime. The results shown in the table indicate that *S* increases with doping in the GaInAsSb layer. These changes are related to the accumulation of electrons near the GaSb/GaInAsSb interface.

Viewgraph 37:

This viewgraph shows the most recent minority carrier lifetime results. In these samples, the growth procedures were modified to minimize growth interruptions at the heterointerfaces, and S has recently been measured to be as low as 30 cm/s

TPV Device Considerations

- **Surface/interface recombination velocity**
  - Interface quality influenced by epitaxial growth process
  - Band alignment at p-GaInAsSb/p-GaSb and p-GaInAsSb/p-AlGaAsSb/p-GaSb interfaces
  - Type-II valence band lineup at GaInAsSb/GaSb interface
  - Flat valence band lineup at GaInAsSb/AlGaAsSb interface
  - Eliminate spikes at heterointerfaces by either AlGaAsSb window layer or by compositional grading/doping: reduce carrier trapping and series resistance
- **Enhancement of minority carrier lifetime with photon recycling**
  - Back surface reflector
  - Integrated distributed Bragg reflector
- **Device fabrication to maximize fill factor**
  - Low series resistance contacts
  - High shunt resistance

Viewgraph 38:

The SRV is a measure of the interface quality and should be minimized to increase quantum efficiency and reduce dark currents. Interface quality can be extremely sensitive to the epitaxial growth procedures. Growth studies revealed that the GaInAsSb surface is reactive at the growth temperature, but it can be stabilized under proper conditions.

Although SRV is not a fundamental property, it can also be affected by band alignment at the GaInAsSb/GaSb or GaInAsSb/AlGaAsSb interface. Type-II alignment in the p-GaInAsSb/p-GaSb interface results in a barrier to majority carrier transport and may also increase series resistance of the device. The valence bands can be lined up for the GaInAsSb/AlGaAsSb interface. Current work is underway to evaluate the subtle differences in interface growth and band alignments.

Increases in minority carrier lifetime are beneficial for TPV cell performance, and can be achieved through photon recyling. Two approaches are being studied: the use of either a back surface reflector or an integrated Bragg reflector (DBR). Substrate absorption can reduce the effectiveness of a back surface reflector, while increased series resistance can be problematic with DBR structures. Preliminary results on integrating a DBR with the TPV device are discussed.
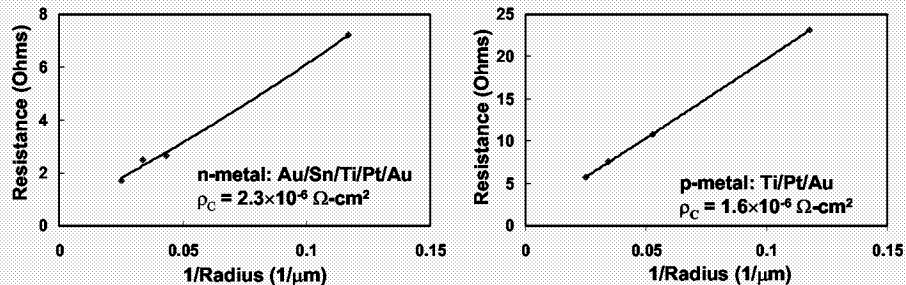
For either approach, low series resistance contacts and high shunt resistance are critical for maximizing the fill factor.

Device Fabrication Development

- **Standard photolithographic fabrication processes**
- **n- and p- metals for low contact resistance**
- **TPV cells defined by wafer sawing**
  - **Saw damage results in low shunt resistance (< 5 Ω)**
  - **Cell walls etched to improve shunt resistance (> 40 Ω)**

Specific Contact Resistivity ρ_C

n-metal: Au/Sn/Ti/Pt/Au
$\rho_C = 2.3 \times 10^{-6}$ Ω-cm^2

p-metal: Ti/Pt/Au
$\rho_C = 1.6 \times 10^{-6}$ Ω-cm^2

TPV-39
CAW 2003

MIT Lincoln Laboratory

Viewgraph 39:

The specific contact resistivity (ohm-cm^2) for both the n- and p-metallization on GaSb was measured by the Cox-Strack method. It was found that both the n and p metallizations were in the low 10^{-6} ohm-cm^2 range. The specific contact resisitivity is slightly lower in the p-metallization than in the n-metallization because the Fermi level is pinned close to the valence band edge in p-GaSb.
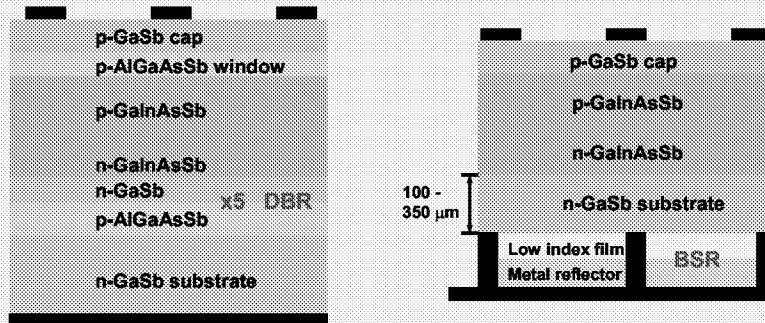
For ease of cell fabrication, individual devices are formed by wafer sawing. The cutting introduces significant damage to the side wall of devices and results in very low shunt resistance and degradation of the fill factor.

Saw-cut damage can be removed with sufficient material etching, as was observed in SEM micrographs of the sidewall before and after etching. The shunt resistance could be increased from a few ohms to hundreds of ohms, while the fill factors increased from below 60% to 70%.

TPV Device Structure Improvements

- **Back surface reflectors (BSR) to increase effective optical thickness and enhance photon recycling**
  - Improve long wavelength spectral response, V_{oc}
- **BSRs on n-GaSb limited by free-carrier absorption**
- **Integrated distributed Bragg reflector (DBR): narrow band**

p-GaSb cap
p-AlGaAsSb window
p-GaInAsSb
n-GaInAsSb
n-GaSb   x5 DBR
p-AlGaAsSb
n-GaSb substrate

100 - 350 μm

p-GaSb cap
p-GaInAsSb
n-GaInAsSb
n-GaSb substrate
Low index film
Metal reflector   BSR

TPV-40
CAW 2003

MIT Lincoln Laboratory

Viewgraph 40:

Two approaches for improving TPV cell performance use a reflector structure, and are shown in this viewgraph. It is expected that the reflector will increase minority carrier lifetime through photon recyling and will provide double-pass absorption for photons that are not absorbed in the first pass. The approach on the left incorporates and integral quarter-wave distributed Bragg reflector (DBR), while the approach on the right is a hybrid ohmic contact back-surface reflector (BSR) deposited on the back of the GaSb substrate. The DBR is more growth intensive, while the and BSR is more fabrication intensive.
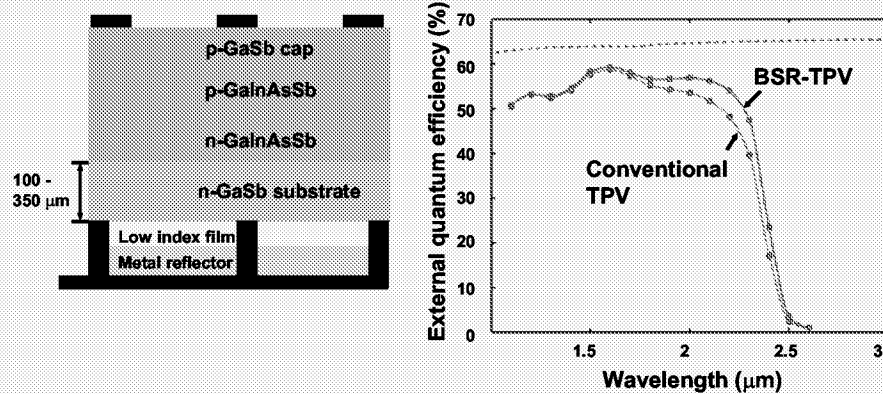
Viewgraph 41:

The EQE of an uncoated BSR-TPV device with substrate thickness of about 120 microns is shown on the left graph. For comparison, the EQE of a conventionally processed TPV cell from the same is also shown. The solid lines are guides for the eyes. The reflection limit of GaSb is also shown, in the dotted-dashed line. In the wavelength regime from about 1.1-μm to 1.7-μm, the BSR-TPV cell and the reference cell have approximately the same EQE since the GaSb substrate is absorbing below 1.7 μm. From about 1.7-μm to 2.5-μm, the EQE of the BSR-TPV cell exceeds that of the reference cell, and indicates the enhancement due to the double-pass absorption. This comparison is made more clear in the graph on the right, in which the difference in EQE is plotted. This value, $\Delta EQE(\lambda)$ is equal to $EQE_{BSR-TPV}(\lambda)- EQE_{REF-TPV}(\lambda)$, where $EQE_{BSR-TPV}(\lambda)$ and $EQE_{REF-TPV}(\lambda)$ are the external quantum efficiencies of the BSR-TPV cell and the reference TPV cell, respectively. The peak difference in EQE is about 8% at a wavelength of 2.35-μm, which corresponds to a fractional increase in EQE of about 20% at this wavelength.
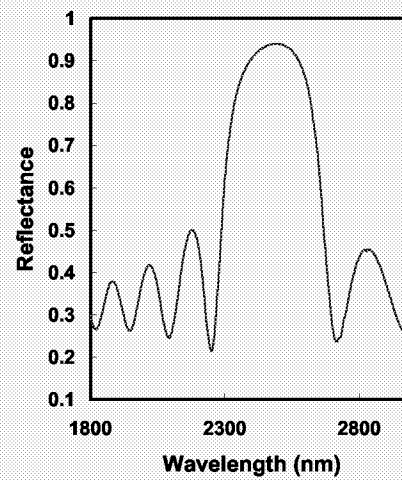
DBR TPV

p-GaSb cap layer
p-AlGaAsSb window layer

p-GaInAsSb emitter layer

n-GaInAsSb base layer
n-GaSb
p-AlGaAsSb   x5   DBR
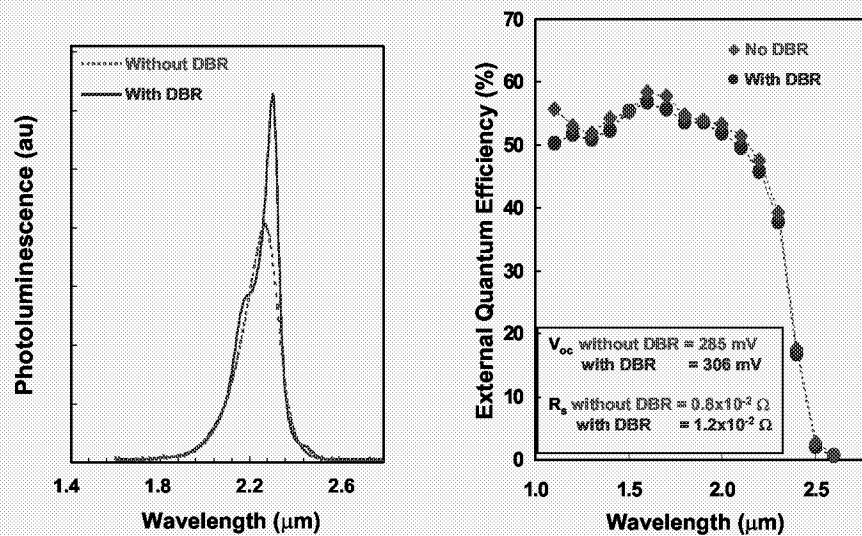n-GaSb buffer layer

n-GaSb substrate

MIT Lincoln Laboratory

TPV-42
CAW 2003

Viewgraph 42:

A TPV device structure was grown with a 5- period DBR structure. The reflectance spectra on the right is for a 10-period DBR. The narrow reflectivity band should enhance the near-band-edge performance.

300 K PL of TPV and DBR/TPV

Viewgraph 43:

The 300 K PL spectra for the TPV control structure and the DBR/TPV structure are compared in this viewgraph. The PL intensity is significantly increased due to photons reflecting off the DBR. The reflectance from the structure with the DBR increases by about 40%.

The EQE of the uncoated TPV and DBR/TPV structures shows similar performance, since the reflection is centered at 2400 nm. It is expected that increased efficiency may be obtained for reflection centered at 2000 nm. The V_{oc} increased by about 7%. Assuming no other changes in the device parameters, the photon recyling factor is estimated to be about 2.5.

The series resistance for the TPV cell with the DBR is slightly higher. Grading the interfaces in the DBR structure should reduce the series resistance.

Monolithically Series-Interconnected Wafer-Bonded GaInAsSb TPV Cells with BSR
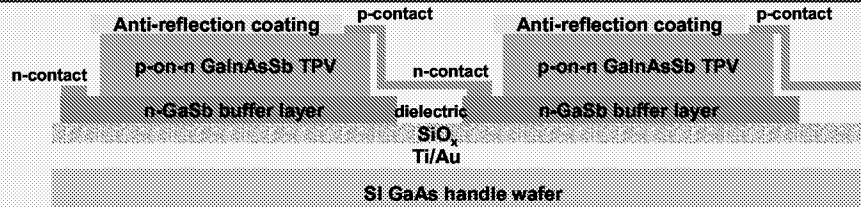
- Wafer bond and transfer GaSb-based epilayers to GaAs
  - SiO_x/Ti/Au bonding layer is multi-purpose
- Broad-band back-surface reflector (BSR)
  - Aids in spectral control
  - Enhances photon recycling
  - Increases optical thickness
- SiO_x allows monolithic series interconnection
  - High-voltage/low-current operation reduces I^2R losses
  - Simplifies fabrication and assembly
- Conducting GaSb substrate precludes monolithic interconnections and free carrier absorption limits effectiveness of BSR
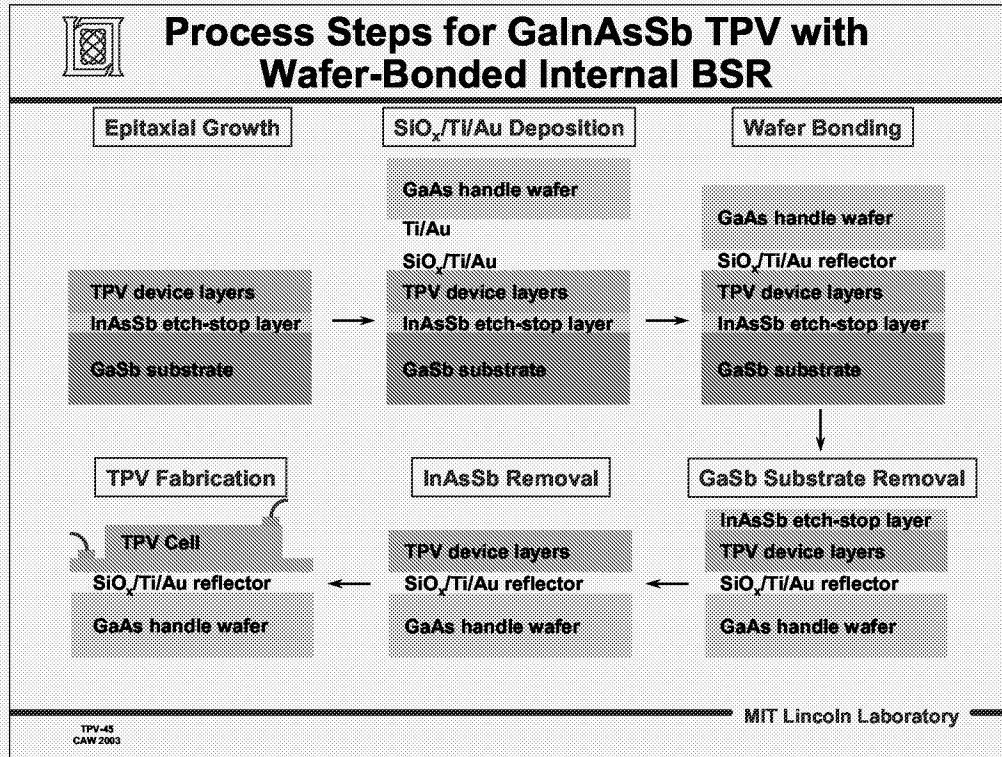
TPV-44
CAW 2003

Viewgraph 44:

It may also be of interest to monolithically integrate TPV devices and connect them in series, as is being done for InGaAs/InP devices. Such an approach requires that the epitaxial structure be on an electrically insulating substrate. Since GaSb substrates can not be made electrically insulating at room temperature, alternative approaches are required.

Two possible approaches are 1) growth on an isolation layer or cell isolation diode and 2) epitaxial layer transfer to an insulating substrate. The second approach is schematically shown. There are several variations to this approach in which the bonding layer can be an oxide, metal, or composite oxide/metal layer. Alternatively, a bonding layer is not used and the GaSb is atomically bonded to GaSb. In this case, the TPV structure would be grown on an atomically bonded GaSb 'buffer' layer.

At present, device processing for monolithic integration has to be refined, while electrical isolation approaches are being developed.

Process Steps for GaInAsSb TPV with Wafer-Bonded Internal BSR

Epitaxial Growth

| TPV device layers |
| InAsSb etch-stop layer |
| GaSb substrate |

→

SiO$_x$/Ti/Au Deposition

| GaAs handle wafer |
| Ti/Au |
| SiO$_x$/Ti/Au |
| TPV device layers |
| InAsSb etch-stop layer |
| GaSb substrate |

→

Wafer Bonding

| GaAs handle wafer |
| SiO$_x$/Ti/Au reflector |
| TPV device layers |
| InAsSb etch-stop layer |
| GaSb substrate |

↓

TPV Fabrication

| TPV Cell |
| SiO$_x$/Ti/Au reflector |
| GaAs handle wafer |

←

InAsSb Removal

| TPV device layers |
| SiO$_x$/Ti/Au reflector |
| GaAs handle wafer |

←

GaSb Substrate Removal

| InAsSb etch-stop layer |
| TPV device layers |
| SiO$_x$/Ti/Au reflector |
| GaAs handle wafer |

TPV-45
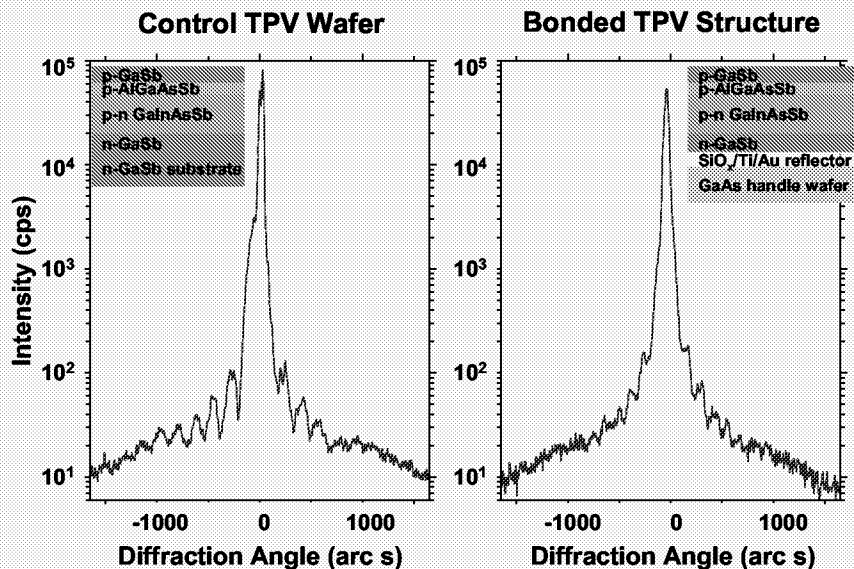CAW 2003

MIT Lincoln Laboratory

Viewgraph 45:

The process steps for fabrication of wafer-bonded TPV devices is shown in this viewgraph. We recently have developed the complete process, and will present results of the materials and devices.

X-ray Characterization of Control and Wafer-Bonded Structures

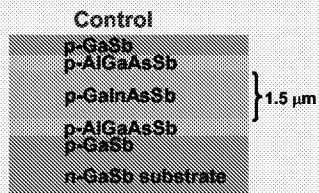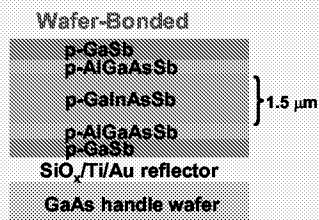Control TPV Wafer — Bonded TPV Structure

TPV-46
CAW 2003

MIT Lincoln Laboratory

Viewgraph 46:

This viewgraph shows a comparison of the XRD rocking curves for a control TPV wafer and a wafer-bonded TPV structure. The diffraction intensity is lower for the bonded TPV device structure since the GaSb substrate has been removed and only the epitaxial layers that were grown lattice-matched to GaSb are remaining. The diffraction peak of the bonded epitaxy is only slightly broadened with full-width at half-maximum (FWHM) of 51 arc s, compared to that of the control structure with FWHM of ~30 arc s. The observation of thickness fringes in both samples is indicative of the excellent structural quality and minimal wafer curvature.
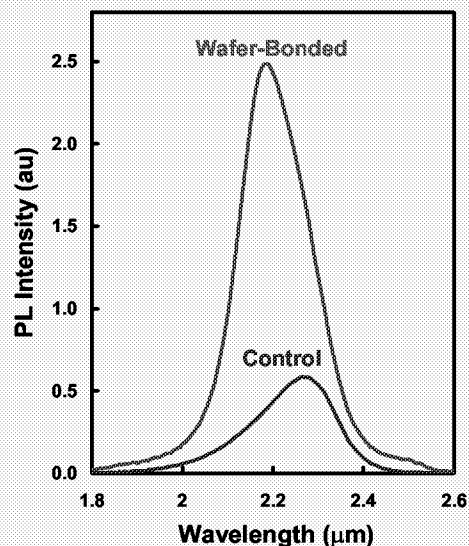
Viewgraph 47:

A comparison of the 300 K PL intensity of a control and wafer-bonded lifetime structure are shown in this viewgraph. The PL peak intensity of the wafer-bonded structure with the internal BSR is almost five times greater than that of the control structure. These results suggest that the optical efficiency is enhanced as a result of the internal BSR, and thus there is negligible material degradation after wafer bonding and substrate removal.
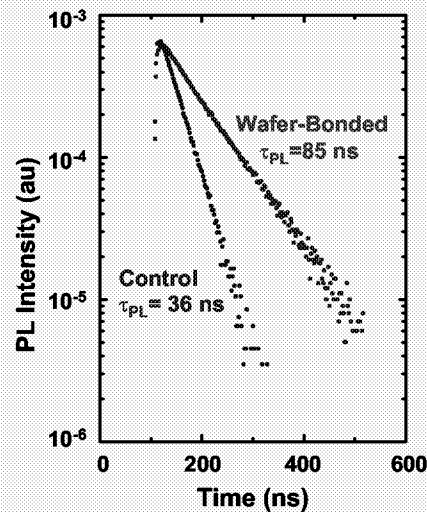
$1/\tau_{PL} = 1/\tau_{NR} + Bp/\phi + 2S/W$

$B \sim 5\times10^{-11}$ cm^3/s; $p = 2\times10^{17}$ cm^{-3}

$S \sim 1300$ cm/s; $W = 1.5$ μm

ϕ = photon recycling factor ~ 3.5

- Benefits of BSR confirmed: higher PL efficiency and higher lifetime of wafer-bonded GaInAsSb
- Optical properties improved for wafer-bonded epitaxy

Wafer-Bonded τ_{PL} =85 ns

Control τ_{PL} = 36 ns

PL Intensity (au)

Time (ns)

TPV-48
CAW 2003

MIT Lincoln Laboratory

Viewgraph 48:

Time-resolved photoluminescence measurements were made to extract minority-carrier lifetime of p-GaInAsSb doubly capped with AlGaAsSb. The lifetime measured by PL decay is more than two times higher at 85 ns for the WB sample with the internal BSR compared to the control sample with decay time of 40 ns. These results show that photons that might normally be absorbed in the substrate are reflected back to the active layer and reabsorbed, and the internal BSR is effective in increasing minority-carrier lifetime. The minority carrier lifetime was also compared. The enhancement in lifetime for the wafer-bonded sample is indicative of the enhancements due to photon recycling.

External Quantum Efficiency of Wafer-Bonded 0.54-eV GaInAsSb TPV Device
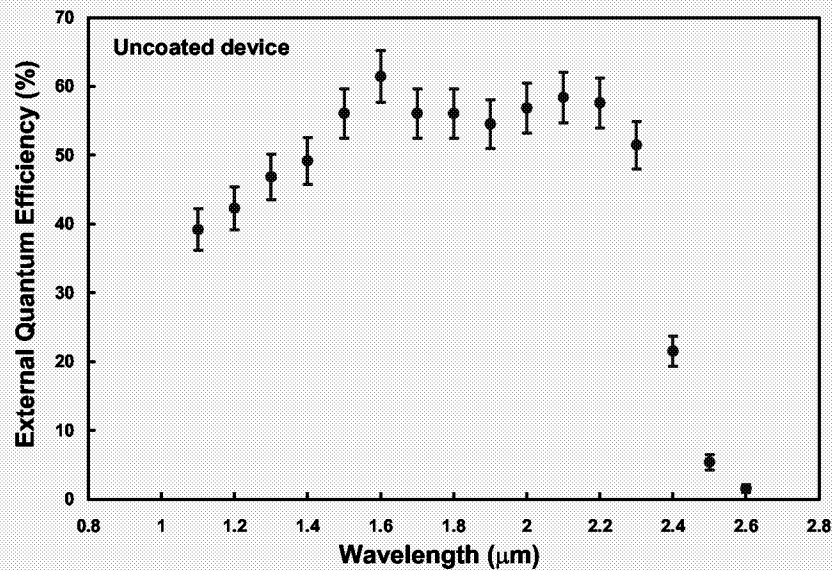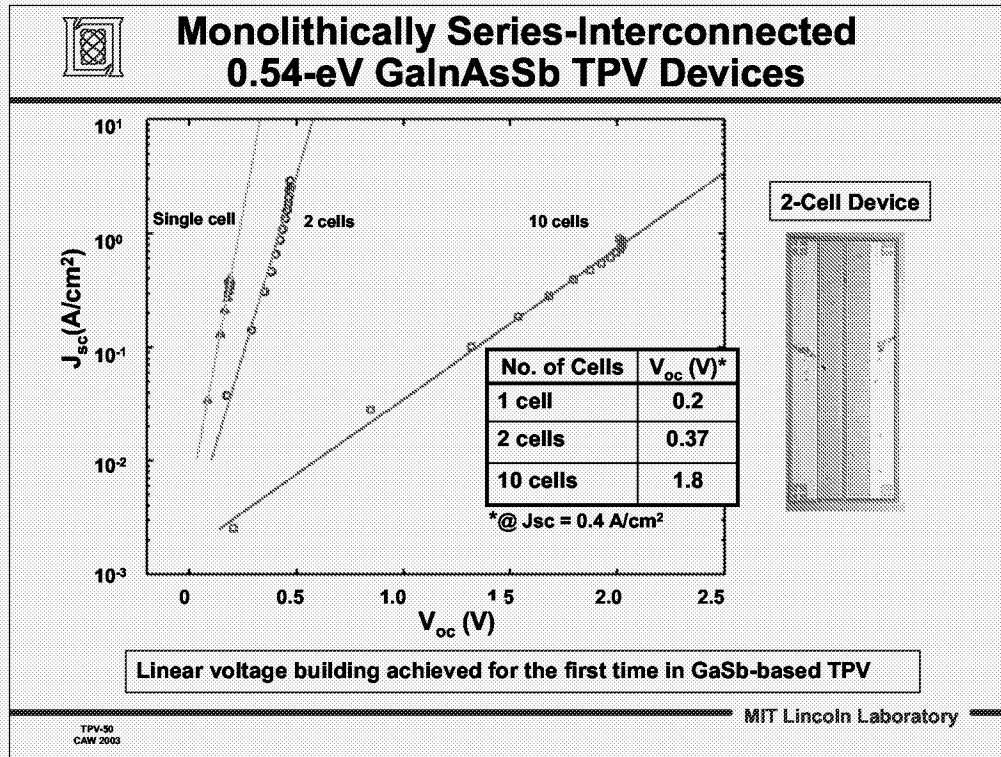
TPV-49
CAW 2003

MIT Lincoln Laboratory

Viewgraph 49:

The external quantum efficiency of a wafer-bonded and uncoated TPV device is shown. The efficiency is slightly lower compared to conventional TPV devices, but is very encouraging nevertheless.

Monolithically Series-Interconnected 0.54-eV GaInAsSb TPV Devices

No. of Cells	V_{oc} (V)*
1 cell	0.2
2 cells	0.37
10 cells	1.8

*@ Jsc = 0.4 A/cm²

2-Cell Device

Linear voltage building achieved for the first time in GaSb-based TPV

MIT Lincoln Laboratory

TPV-50
CAW 2003

Viewgraph 50:

This viewgraph shows the short-circuit current density J_{sc} versus V_{oc} for a single-junction TPV cell and 2- and 10-junction series-interconnected TPV cells that were fabricated on the wafer-bonded material. At $J_{sc} \sim 0.4$ A/cm2, the single cell exhibits $V_{oc} \sim 0.2$ V. At this same current density, V_{oc} is 0.37 and 1.8 V for the 2- and 10-junction devices, respectively. These results indicate that nearly linear voltage building has been achieved. At higher $J_{sc} \sim 1$ A/cm2, V_{oc} is ~ 0.470 and 2.0 V for the 2- and 10-junction devices, respectively. The saturation of V_{oc} at high Jsc levels may be due to heating of the devices, which were not mounted on a heatsink. The V_{oc} for the single cell is slightly lower compared to previously reported values for conventional TPV cells, and is likely related to a higher saturation current. This may stem from the larger cell perimeter/area ratio compared to previously reported cells or from pinholes in the epitaxy due to etching. The fill factor FF of the 2-junction device is about 51% at Jsc ~ 0.4 A/cm2, and degrades to about 38% at Jsc ~ 1 A/cm2. This degradation is related to high series resistance in the cell-to-cell interconnections, and could be reduced with improved metallization and reduced resistance in the n-GaSb lateral conduction layer.

Summary

- **Epitaxial growth and fabrication studies directed toward improving GaInAsSb/AlGaAsSb/GaSb TPV device performance**
- **IQE and FF approaching theoretical limits, V_{oc} within 12%**
- **Back-surface reflector designs evaluated for further enhancements**
    - **Integrated DBR/TPV device exhibits higher open circuit voltage**
    - **TPV with back-surface reflector exhibits higher quantum efficiency near GaInAsSb band edge**
- **Alternative approach by wafer-bonding for monolithic interconnection of GaSb-based TPVs**

TPV-51
CAW 2003

MIT Lincoln Laboratory

Viewgraph 51:

This presentation has discussed the development of GaInAsSb materials and device structures for lattice-matched TPV devices. The performance of TPV cells is approaching theoretical limits. These TPV devices can routinely be fabricated, indicating good control and reproducibility of both epitaxial growth and device processing. Preliminary results on devices with an integral DBR structure indicate an increase in V_{oc}. Improvements in EQE was measured for TPV cells with a BSR. Initial results of wafer-bonded TPV devices are very encouraging.